Modeling sea surface scattering by the time-domain finite-difference method

Ralph A. Stephen
Woods Hole Oceanographic Institution, Woods Hole, Massachusetts 02543

(Received 22 June 1995; accepted for publication 14 February 1996)

A numerical scattering chamber based on the time-domain finite-difference solution of the two-way elastic wave equation is applied to a sea surface scattering problem, and excellent agreement is obtained in amplitude and phase with a reference solution obtained by an integral equation method. The sea surface roughness is one representation of a Pierson–Moskowitz spectrum for a wind speed of 15 m/s. The incident field is a 400-Hz continuous wave generated by a Gaussian tapered vertical array. This problem demonstrates a number of issues in numerical modeling of wave scattering. The spreading of Gaussian beams, even in homogeneous media, creates an asymmetry in the insonification of the surface footprint or scattering area. Because of beamspreading, Gaussian tapered vertical arrays do not generate Gaussian beams. Scattering from a rough, free, fluid surface can be accurately solved with careful treatment of the numerical boundary representing the free surface. Continuous wave (cw) scattering problems can be solved in the time domain. For the second-order, explicit, staggered finite-difference formulation used in this study, a spatial sampling of 20 points per acoustic wavelength was necessary for acceptable grid dispersion. However, to correctly compute the scattered field for the test model, it was sufficient to specify the free surface at a spatial sampling of only ten points per acoustic wavelength.

PACS numbers: 43.30.Gv, 43.30.Hw, 43.20.Bi, 43.20.Fn [JHM]

INTRODUCTION

Time-domain finite-difference modeling of the two-way elastic wave equation has proven to be a useful tool in bottom interaction studies where it includes complete compressional and shear-wave effects and all multiple interactions between body and interface waves (Dougherty and Stephen, 1988; Dougherty and Stephen, 1991; Levander *et al.*, 1993; Orcutt *et al.*, 1993; Swift and Stephen, 1994). The technique can be applied as well to sea surface scattering problems where it can provide additional insight into scattering processes that is not given by other methods. Our approach, which we refer to as a numerical scattering chamber (NSC), is discussed in detail by Stephen and Swift (1994b). In this paper we present our solution to a reference model proposed by Thorsos (1996), a sea surface scattering example, and discuss some significant issues that arise in the modeling.

I. BACKGROUND

A. A time-domain finite-difference method for cw acoustic scattering problems

A numerical scattering chamber (NSC) for seafloor problems, based on the elastic wave equation, is described by Stephen and Swift (1994b). In the Appendix to their paper they show how the elastic formulation reduces to the acoustic formulation by simply setting the shear modulus to zero everywhere in the model. In this approach losses in the fluid can be considered, as demonstrated by Stephen and Swift (1994a). Stephen (1990) shows that a stress release boundary condition can be adequately represented in this formulation by setting the compressional velocity to a very low value while keeping the density constant for grid points outside of the fluid. In this manner arbitrarily shaped rough free surfaces can be treated in the NSC.

Although the code solves wave equations in the time domain, cw sources can be treated by using a single-frequency, continuous, sinusoidal source waveform and running the code until steady state is reached. This was the approach taken by Stephen (1990) for the Acoustical Society of America benchmark wedge models. A window of data from each pressure time series is acquired after steady state is reached. Amplitudes and phases of the resultant field are obtained from the transfer function with the source field.

B. Gaussian beams

This sea surface scattering problem uses a Gaussian beam for the incident field and is consistent with the NSC methodology developed for seafloor scattering problems (Stephen and Swift, 1994b). Gaussian beams are a useful way to restrict the angular (or horizontal wave number) content of the incident field while keeping the interaction localized on the surface (Červený *et al.*, 1982; Chimenti *et al.*, 1994; Felsen, 1976; Thorsos, 1988). However, by truncating a plane wave the additional complexity of beamspreading (Huygen's principle) must be considered. This introduces propagation issues into scattering problems.

Červený *et al.* (1982) discusses the computation of wave fields using Gaussian beams. The center or peak amplitude of the beam follows a ray path with distance along the path, s. The profile of the beam is Gaussian with a half-width (the width to the point where the amplitude decreases to e^{-1} of the peak value), L. Beamspreading is described by $L(s)$, which for a homogeneous medium is

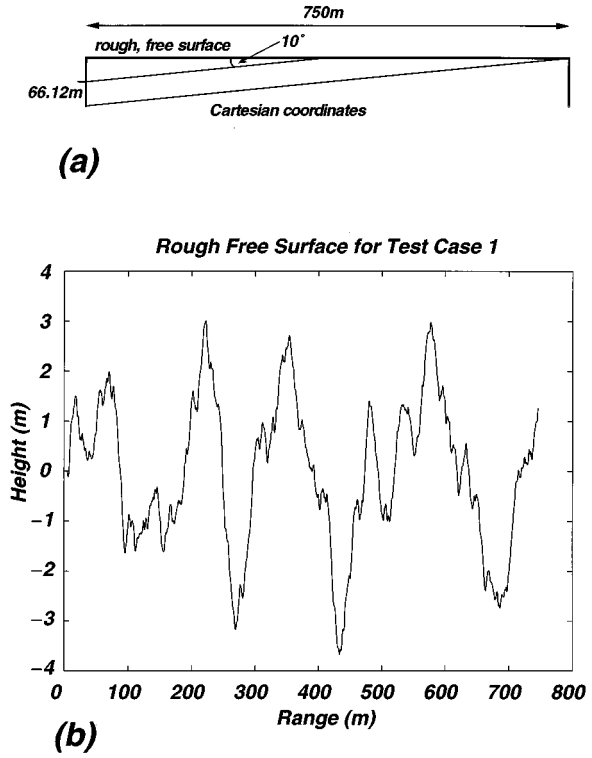

FIG. 1. The model consists of a 400-Hz cw beam propagating from a Gaussian tapered vertical array on the left side which is steered to insonify the free surface at a grazing angle of 10° (a). The total field is observed on a vertical array on the right side at a range of 750 m. The rough free surface is a one-dimensional representation of a Pierson–Moskowitz spectrum for a wind speed of 15 m/s (b). This model fits conveniently into the numerical scattering chamber (Stephen and Swift, 1994b).

$$L(s)=\left[L_M^2+\left(\frac{2v_0}{\omega L_M}\right)^2(s-s_0)^2\right]^{1/2}, \tag{1}$$

where L_M is the minimum half-width of the beam which occurs at path distance, s_0; v_0 is the velocity of the medium; and ω is angular frequency. For a given path length, $(s-s_0)$, there is an optimal initial beam width, L_M^{opt}, which will yield the narrowest beam. For homogeneous media this width is

$$L_M^{\text{opt}}=\left[\frac{2v_0}{\omega}(s-s_0)\right]^{1/2}. \tag{2}$$

When applying Gaussian beams to interface scattering problems, the smallest footprint on the interface will correspond to the narrowest beam.

II. AN EXAMPLE OF SEA SURFACE SCATTERING

A. The model and solution

To demonstrate the application of the numerical scattering chamber to sea surface scattering problems we consider the benchmark model proposed by Thorsos (1996). The model is defined in a two-dimensional Cartesian geometry (Fig. 1). A 400-Hz, continuous wave, Gaussian tapered, continuous vertical array at zero range is phased to create a tapered planar wavefront which is incident on the sea surface at a grazing angle of 10°. The Gaussian profile has a peak value at 66.12-m depth at zero range and an initial half-width

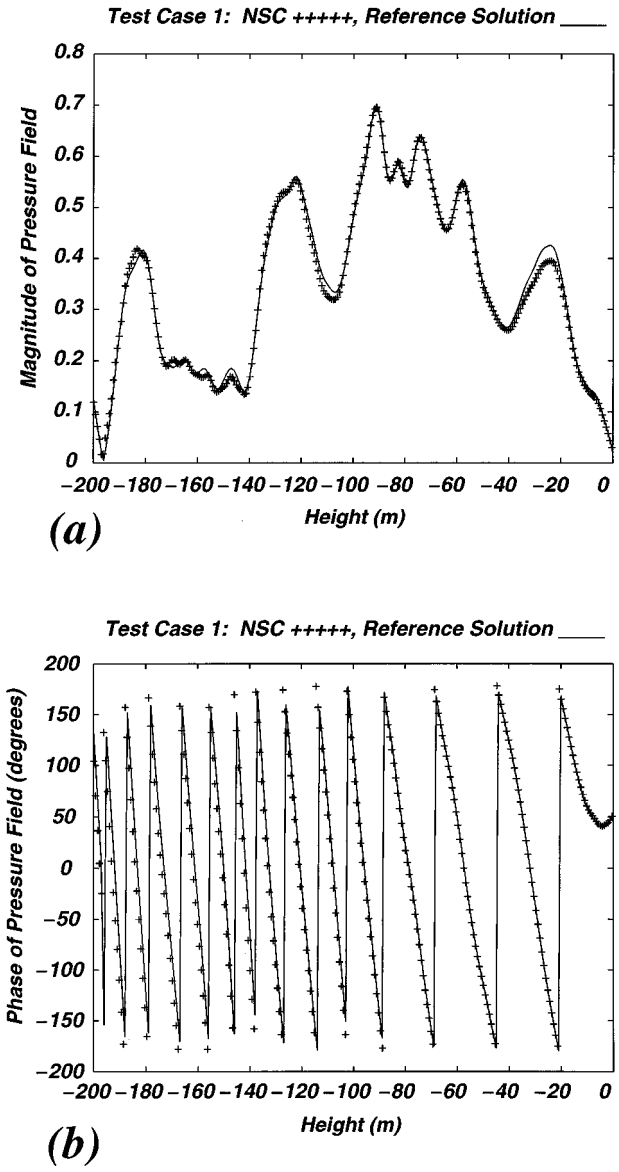

FIG. 2. The amplitude and phase [(a) and (b), respectively] of the finite-difference solution (crosses) agree well with the integral equation solution (solid) which was provided by Thorsos (1996).

of 27.55 m. The full field is computed as a function of depth at a range of 750 m. The medium below the free surface is homogeneous water with a compressional velocity (V_p) of 1.5 k/s and a density of 10^3 kg/m^3. The rough free surface is a one-dimensional representation of a Pierson–Moskowitz spectrum for a wind speed of 15 m/s (Pierson and Moskowitz, 1964). The free surface representation has been sampled at ten points per wavelength (ppw). The reference solution was computed using an exact integral equation method (Thorsos, 1988).

The amplitude and phase of the NSC solution to this problem are compared with the reference solution in Fig. 2. Amplitude and phase were computed from the continuous wave output of the NSC by transfer function estimation. The transfer function was computed as the ratio of the cross spectrum of a given trace with the reference, zero-phase, trace,

and the power spectrum of the reference trace (Krauss *et al.*, 1993). As defined in the test case specifications, the reference, zero-phase trace is the incident field on the left-hand side at $z=0$. Also, the amplitudes are normalized so that the peak pressure of the incident field defined on the left-hand side is unity.

Good agreement between the NSC solution and the reference solution is obtained. The solutions agree to within 1 dB in amplitude and to within 46° (an eighth of a period) in phase except in the steep notch between 193 and 198 m. The phase of the reference solution has a discontinuity in slope at 196 m, which is not observed in the NSC solution. We have no physical explanation for the discontinuity and suspect that the reference solution may be incorrect in this region. Although the maximum discrepancy in phase is quite large (46°) the mean deviation from the surface down to 193 m is only 13° (less than a twenty-fifth of a period).

B. Finite-difference modeling

1. Grid dispersion

In the scattering problem defined above there are both scattering and propagation effects. Since the incident field is not uniform with range across the surface, the scattered field will depend on where the scattering elements are within the incident field. This restricts the generality of scattering results obtained by incident beam methods. It also makes it important to correctly model the propagation from the source array to the interface and from the interface back to the receiver array, even when the source and receiver arrays are only a few hundred wavelengths apart.

In the NSC the finite-difference method is used to propagate the field through homogeneous portions of the model, even though exact analytic Green's functions exist. An inherent problem with all finite-difference and finite-element methods for directly solving wave equations is grid dispersion. The numerical velocity of propagation across the grid depends on the number of grid points per wavelength (Alford *et al.*, 1974), and the accuracy of a solution will depend on the propagation distance (Dablain, 1986). It is worthwhile considering just the propagation portion of the benchmark problem to ensure that grid dispersion issues are correctly handled.

For the 20-ppw model, we use $\Delta t=8.333\times10^{-5}$ s and $\Delta x=\Delta z=0.1875$ m. This gives a Courant number $(V_p\Delta t/\Delta x)$ of 0.667. The theoretical maximum Courant number for stability of the staggered grid scheme we are using is 1/sqrt(2) or 0.707 (Virieux, 1986). For a fixed grid step interval and velocity, we choose the time step interval to give a convenient number of samples per second for plotting and processing. Since grid dispersion is minimized when the Courant number approaches the stability limit, our Courant number is not optimal for grid dispersion. The difference in normalized phase velocity, at 20 ppw and an angle with the grid of 10°, between Courant numbers of 0.667 and 0.707 is 0.02%, which is negligible. However, the additional computational effort in using a smaller time step than necessary is about 5%.

For acoustic propagation in fluids there are second-order centered schemes which are stable for Courant numbers up to unity (Bamberger *et al.*, 1980; Stephen, 1983, for example). These would allow for coarser time steps and an improvement in computation time of about 33%. However, the code that we are using for this study was developed for bottom scattering and includes the capability for shear-wave effects. In the case of elastic interactions (with shear), the staggered grid scheme has uniform dispersion and stability properties over the complete range of Poisson's ratios and is preferred to the centered grid schemes (Virieux, 1986). The code we are using in this case is not optimal for sea surface scattering, but it is reassuring to know that a code developed for bottom scattering from elastic media also gives accurate solutions for the sea surface case.

If we just want to propagate sound in homogeneous water we could use higher-order schemes which permit comparable accuracy and stability for coarser grids (Alford *et al.*, 1974; Dablain, 1986). But if we need a certain grid interval, say 20 ppw, to adequately represent the surface for the scattering problem, then we cannot take advantage of the coarser grid option. Since the computational effort per time step is more involved and since the stability criteria requires finer time steps, higher-order schemes are at a disadvantage over second-order schemes for the same grid size.

As a numerical test of the effects of grid dispersion in our code, we consider the incident field only on the right-hand side of Fig. 1 without the effects of the sea surface. Figure 3 shows the solution computed by the NSC at two discretization levels and the reference solution computed by an integral equation method by Thorsos (1996). The two discretization levels are 10 ppw in space [15 ppp (points per period) in time] and 20 ppw in space (30 ppp in time).

The NSC amplitudes are shown in Fig. 3(a). Clearly 20 ppw gives a better result than 10 ppw. The discrepancy between 20 ppw and the reference solution is less than 1.5 dB down to levels of -75 dB below the peak incident field level which occurs at a depth of 57 m. The maximum discrepancy for the 10-ppw case over the same interval is 5.6 dB. The NSC phases are shown in Fig. 3(b). Below 57-m depth, where the amplitudes are less than -75 dB below the peak incident field level, both the 10- and 20-ppw solutions have considerable discrepancies with respect to the reference solution. We attribute this to numerical noise and truncation effects in the finite-difference calculations. (At these depths, because of the spreading of the incident beam, the energy is actually arriving at the right-hand vertical array from above.) Above 57-m depth, the maximum phase errors are 42.8° and 15.0° for the 10-ppw and 20-ppw solutions, respectively, and the mean phase errors are 27.0° and 2.3°, respectively. The 10-ppw phases are unacceptable with a mean phase error of almost a twelfth of a period, but the 20-ppw phases are acceptable with a mean phase error less than a hundredth of a period. It is quite clear that, using the second-order staggered finite-difference scheme (Stephen and Swift, 1994b; Virieux, 1986), adequate accuracy over propagation ranges of 200 wavelengths requires sampling at 20 ppw or more.

The numerical test is a better measure of the accuracy of the NSC calculation than simply applying the dispersion cri-

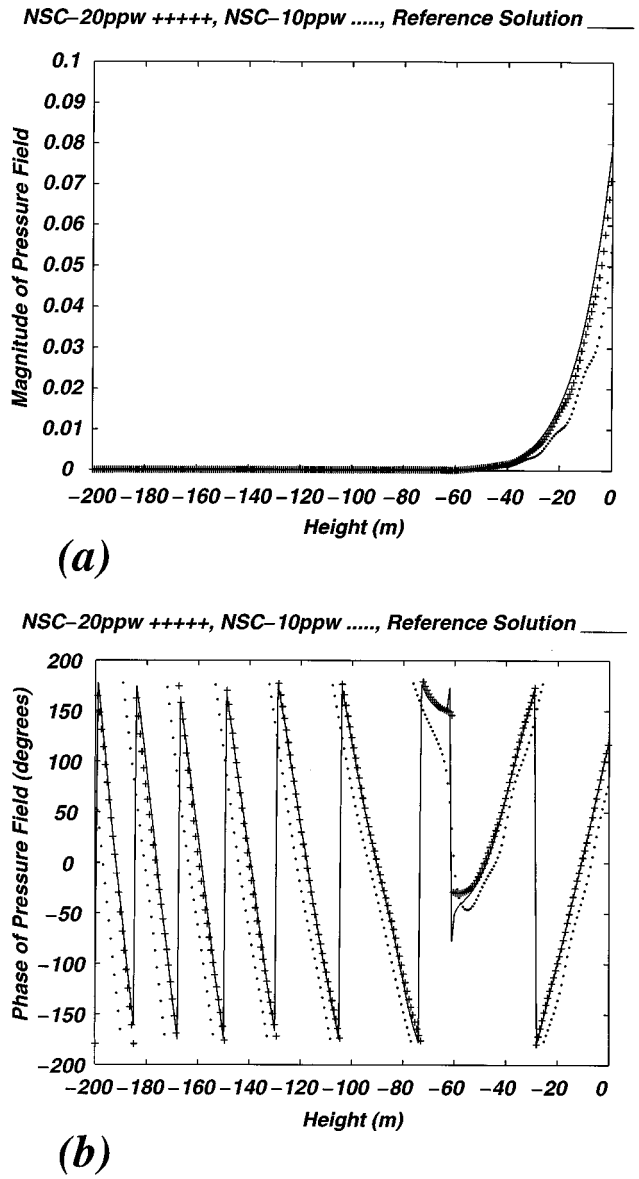

FIG. 3. In order to check for grid dispersion, the finite-difference solution at 10 and 20 grid points per wavelength (dots and crosses, respectively) is compared with the integral equation solution (solid line) for the incident field only, without reflections or scattering. Ten points per wavelength for a second-order scheme is a frequently used rule of thumb, but it can be seen from the figure that 20 points per wavelength gives a much better result for this problem.

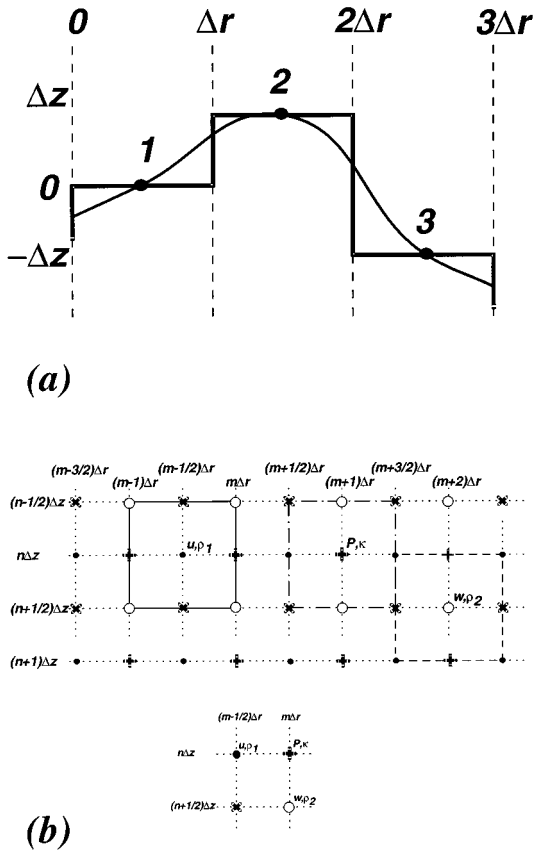

FIG. 4. Finite-difference methods are sensitive to the manner in which material properties are defined on the discrete grid. One continuous sea surface profile that could be represented by the first three discrete wave-heights is shown with a curved line (a). The stepwise curve shows one way in which these three values could be interpreted on a discrete grid. If the intervals Δr and Δz are small enough with respect to a wavelength, these two representations would give the same scattering result. The definition of our staggered grid (Stephen, 1990) is also shown (b). The compressibility (κ), density (ρ_1 and ρ_2), horizontal and vertical displacement (u and w), and pressure (P) are defined on the staggered grid in a fashion analogous to Virieux (1986). One consequence of a staggered grid is that the cells overlap and literal interpretation of cell boundaries is physically impossible.

teria. The numerical test includes the effects of beamspreading and it includes amplitude effects as well as phase effects. Based on the dispersion criteria for a plane wave at 10° grazing angle (Alford *et al.*, 1974), the predicted phase errors of a 400-Hz wave over 761 m (the slant range from the vertical array to the surface) are 605° and 144°, respectively. These predictions exceed considerably our computed phase errors based on the reference solution for the incident beam.

2. Discretizing the rough sea surface

The Pierson–Moskowitz representation of the sea surface used for the reference solution gives sea surface height to a resolution of a millimeter ($\lambda/3750$) or less at points separated by 0.375 m ($\lambda/10$) (where λ is wavelength). The NSC uses a uniformly spaced grid at 20 ppw. Two questions arise: Is there any point in specifying the sea surface height at better than $\lambda/20$? What is the correct way to interpolate points at 10 ppw to points at 20 ppw, or does it matter?

Figure 4(a) shows one interpretation of the digital height values given for this test case. Values are given corresponding to the center of cells that are a tenth of a wavelength wide. Presumably, the heights are samples of a continuous function and we hope that the acoustic response of the stair-step interpretation is equivalent to the continuous case.

Our finite-difference scheme is based on the staggered grid formulation of Virieux [1986, Eq. (2)], but rather than using a velocity–stress–buoyancy formulation we use a displacement–density formulation [Stephen, 1990, Eq. (1)]. The velocity–stress–buoyancy formulation solves a system of first-order equations with only first derivatives in time and space. The displacement–density formulation solves the second-order wave equation in terms of displacement di-

rectly with second derivatives in time. The spatial derivatives of displacements are computed by two applications of first derivatives using stress as an intermediate variable. Spatial derivatives of the Lamé's parameters are not taken explicitly.

The formulation used for this acoustic test problem is identical to the elastic formulation (Stephen, 1990; Stephen and Swift, 1994a; Stephen and Swift, 1994b) except that shear velocities and shear stresses have been set to zero. Pressure is computed from the displacements in postprocessing. The staggered scheme is shown in Fig. 4(b). This is the same as Fig. 1 in Stephen (1990) with the shear velocity and stresses removed and Lamé's parameter, λ, set to the bulk modulus, κ.

One consequence of a staggered grid scheme is that the cells corresponding to various field variables and parameters overlap, as shown in Fig. 4(b). Literal interpretation of the cell boundaries is physically impossible. For example, the cell for density, ρ_1, used to compute horizontal displacement, overlaps the cell for density, ρ_2, used to compute vertical displacement. Some smoothing, over distances much smaller than a wavelength, is implied in the formulation.

Our algorithm for assigning parameters to the finite-difference cells consists of three steps: (1) Subdivide the range data from $\lambda/10$, given in the problem, to $\lambda/20$, as required by the finite-difference scheme; (2) Assign an interface height to each range point. Heights in the finite-difference scheme are also quantized in $\lambda/20$ units, so rounding is required from the data values given at $\lambda/3750$. For ranges which match the given data exactly, only rounding is performed. For the interpolated ranges, it is assumed that the height is the same as at the given range to the left. This gives a coarse step (10 ppw) representation of the surface; (3) Smooth the parameters to allow for the overlapping grid cells, as described below.

Figure 5 shows the cell assignments for the κ, ρ_1, and ρ_2 cells. Zero range and height are chosen to fall in the center of a κ cell. (P is pressure and κ is bulk modulus.) So, for the first cell, horizontal displacement and density, ρ_1, are at negative range. We also choose the literal boundary to occur between κ cells. This has the effect of shifting the interface $\lambda/40$ further to the right from the source and $\lambda/40$ deeper as shown. In order for the ρ_1 and ρ_2 cells to be consistent with the boundary between the κ cells, it is necessary to average values vertically for ρ_1 and horizontally for ρ_2. As mentioned above, for this test case we represented the free surface as a discontinuity between compressional velocities of 1.5 km/s and 10^{-8} km/s while keeping density constant. In this case, the averaging of density is inconsequential and the numerical free surface is located at the κ cell boundaries without smoothing. We obtained such good agreement to the reference solution for this scheme that we did not investigate other schemes. Note that the free surface condition is being handled implicitly by a change in elastic parameters in the wave equation for heterogeneous media. A boundary condition is not explicitly applied.

Figure 6 compares the seaheight in the finite-difference grid with the given seaheight. For finite-difference modeling the given seaheight data was too coarse in range and much too fine in height. Since good solutions were obtained by the

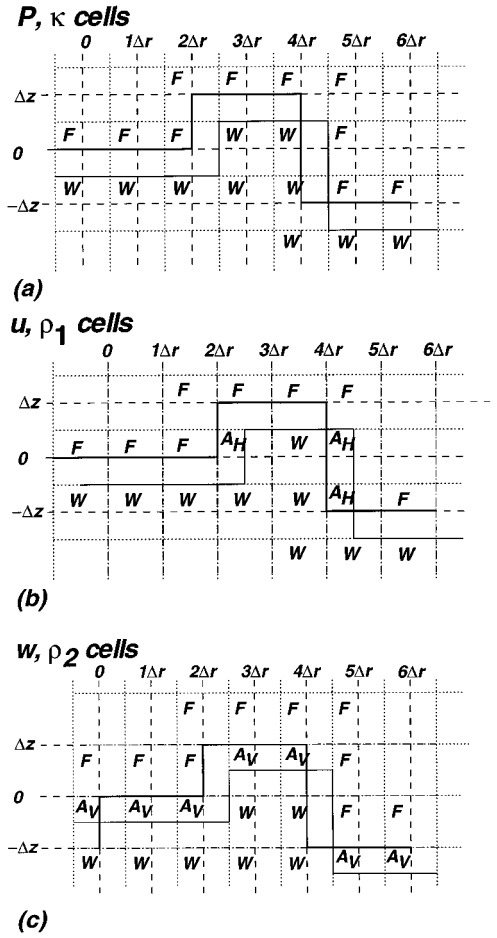

FIG. 5. The cell assignments for κ, ρ_1, and ρ_2 are shown [respectively, (a), (b) and (c)]. Cells marked F have properties of the free medium and cells marked W have properties of water (see text). Cells marked A_V and A_H have properties averaged vertically and horizontally, respectively. The thick line staircase is the location of the nominal rough surface shown in Fig. 4(a). The thin line staircase is the boundary between free and water cells and is offset half a grid increment from the nominal rough surface.

finite-difference grid, it can be concluded, that for acoustic modeling, it is sufficient to specify seaheights to within a twentieth of a wavelength in height.

The Pierson–Moskowitz spectrum in this example has a peak value at a spatial wave number of 0.03 m^{-1} and it has essentially all of its energy at wave numbers less than 0.3 m^{-1}. The acoustic wave number is 1.68 m^{-1} and most of the roughness is occurring over length scales greater than five wavelengths. The Pierson–Moskowitz surface sampled at 20 ppw is the same as a linearly interpolated version of the surface sampled at 10 ppw. We computed the solution at 20 ppw using a linearly interpolated version of the 10-ppw surface, rather than the 10-ppw steps, and obtained identical results. The time-domain finite-difference solution is insensitive to the details of interpolation at scales less than 10 ppw. The surface discretization of 10 ppw for this problem is sufficient as pointed out by Thorsos (1996).

3. Absorbing boundaries

One challenge in time-domain finite-difference methods is to effectively minimize artificial reflections from the edges

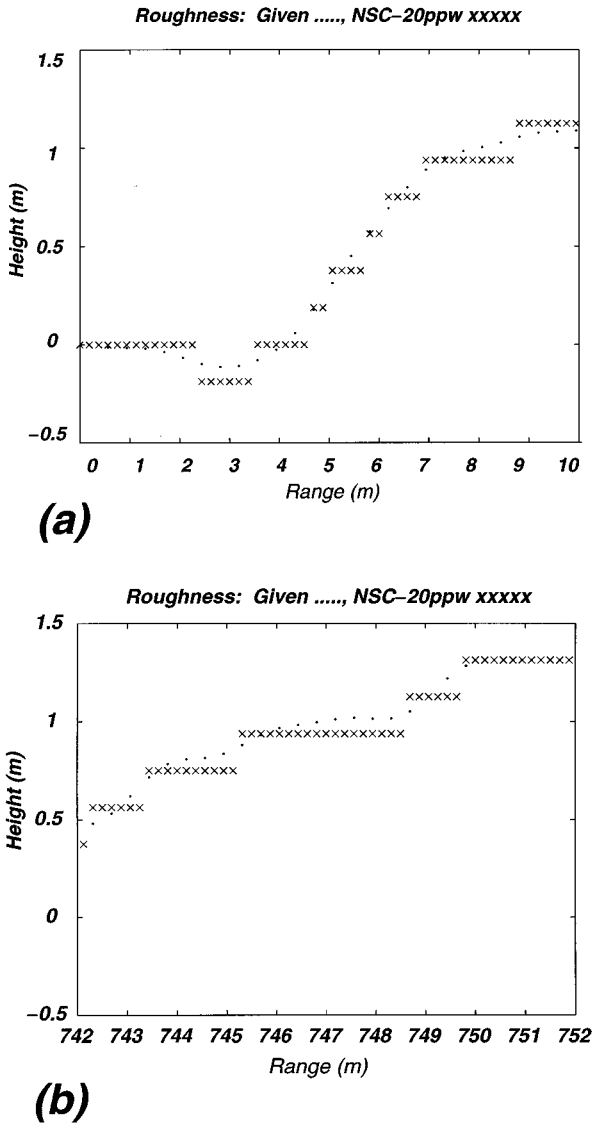

FIG. 6. This figure compares the given seaheight values (dots) to the seaheights in the finite-difference grid (crosses), for two segments of the surface. For finite-difference modeling on a uniform grid, the specified seaheight was too coarse in range and too fine in height.

of the truncated spatial domain. There is extensive literature on this subject which we do not attempt to review here. However, based on our experience two problems arise. Many formulations assume homogeneous media adjacent to the absorbing boundary and focus on absorbing body waves with linear particle motions. In our seafloor studies, Stoneley and pseudo-Rayleigh waves which have elliptical particle motions propagate along the sharp water bottom interface which intersects the absorbing boundaries on the left- and right-hand edges. Many absorbing boundary formulations do not work in this case.

The second problem that occurs is instability at the absorbing boundary at long time durations. The initial body waves are well absorbed, but at long durations, for example the 500 periods required to reach steady state in the finite spatial domain of this example, the absorbing boundary conditions are unstable.

We have addressed both of these problems empirically. The parameters used in this test case are based on our experience with seafloor models and have not been optimized, or even improved, for the sea surface scattering case. Our objective in this study was accuracy, not performance. We use a hybrid absorbing boundary condition based on the telegraph equation approach (Cerjan *et al.*, 1985; Levander, 1985) and a paraxial approximation to the wave equation at the edge of the domain (Higdon, 1991). The telegraph equation is applied in a zone surrounding the domain that is nine wavelengths deep, and the attenuation parameter is increased gradually with penetration into the zone (Stephen, 1990). At the ultimate edge of the grid we use Higdon's second-order boundary condition.

4. Computational performance

The solution in Fig. 2 was computed using a time-domain, elastic, finite-difference code with the shear velocities and stresses set to zero. Overall grid dimensions, including absorbing boundaries, were 4430 points in range and 1223 points in height. The code was run for 7205 time steps. The memory size was 93.3 Mb and the calculation required 9 h and 22 min of CPU time on a DEC Alpha 3000/400 desktop workstation.

C. Discussion of beamspreading

Beamspreading distorts our notion of the incident field in three ways. First, a Gaussian tapered, phased vertical array does not generate a plane wave with a Gaussian profile. The incident field in this test case is not strictly a Gaussian beam. Second, neither the Gaussian tapered vertical array nor a strict Gaussian beam give a Gaussian distribution of amplitude on the horizontal sea surface. Third, even though the incident field is initiated with a planar wavefront, angle spread occurs before the wave hits the interface.

To demonstrate these effects, we consider the same model as defined above but with a flat, stress free, sea surface. Figure 7 shows the amplitude as a function of depth of the source field at $x=0$ and of the received field at $x=750$ m, as computed in the NSC with 20 ppw in space and 30 ppp in time. The beam has clearly spread in propagating across the homogeneous medium. The amplitude of the profile has decreased to about 0.79 of its original value and the half-width has increased from 27.55 to 44.52 m. The total energy in the incident and reflected profiles is identical within 0.01%. The non-Gaussian shape on the right side of the reflected profile is caused by interference with the lower tail of the incident beam, which is not quite negligible at 750-m range [Fig. 3(a)], and by asymmetrical spreading of the beam.

To check the discrepancy introduced by approximating the Gaussian beam with a Gaussian tapered vertical array (Fig. 8), we compare the half-width of the computed reflected beam with the predicted half-width for a corresponding Gaussian beam. The half-width of the vertical Gaussian taper of the incident profile is 27.55 m. If we neglect beamspreading and simply project the vertical profile onto a plane at 10° from vertical, we obtain a corresponding Gaussian beam with a half-width, L_M, of 27.13 m. The propagation

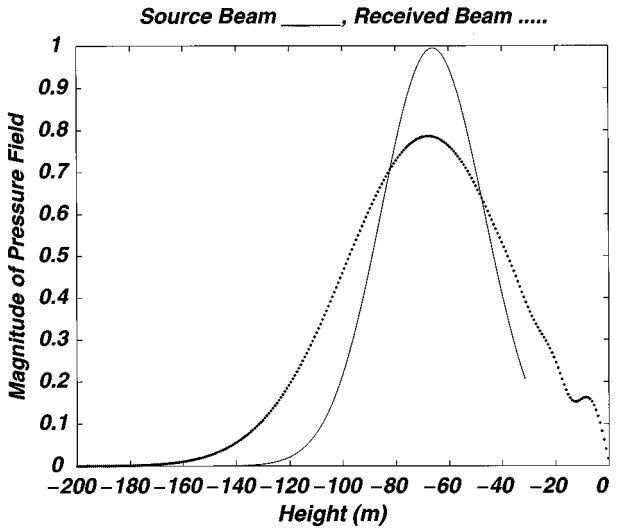

FIG. 7. To demonstrate the effect of beamspreading, we compare the source beam profile (solid) to the received, mostly reflected, beam profile (dotted), for the case of a flat sea surface. In propagating from the source to the receiver arrays (750 m apart) the beam has spread from a half-width of 27.55 m to a half-width of 44.52 m and its amplitude has decreased from 1 to 0.79. The small bump on the right side of the reflected profile is caused by interference with the tail of the incident beam, which is not quite negligible, and by asymmetrical spreading of the beam.

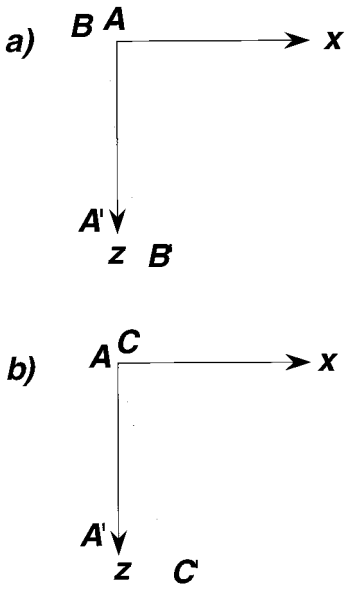

FIG. 8. A Gaussian tapered vertical array does not generate a Gaussian beam. To check the discrepancy we compare the received beam for a flat sea surface using two source configurations. The first configuration is the tapered and phased vertical array defined in the test problem. The observed field at the receiving array is computed by finite differences. The second configuration is the corresponding Gaussian profile along the plane $B-B'$ with the center of the source beam at the range $x=0$ (a). The profile along this plane is obtained by projecting the profile along the vertical array $A-A'$ to the plane $C-C'$ without beamspreading (b). Physically some beamspreading would occur over the propagation path from $A-A'$ to $C-C'$, but this is ignored. The observed field at the receivers is then computed analytically, as discussed in the text. The half-width of the reflected beam from the tapered vertical array is 44.52 m. The half-width of the reflected beam from the corresponding Gaussian beam is 43.11 m, a discrepancy in beamwidth of 1.7%.

pathlength, $(s-s_0)$, is 761.57 m (750/cos 10°), which gives a half-width from Eq. (1) of 43.11 m for the reflected beam at $x=750$ m. The projected profile onto the vertical right-hand axis, that is, the corresponding Gaussian beam, has a half-width of 43.78 m. The measured half-width of the NSC results, that is, from the tapered vertical array, is 44.52 m. In this example, approximating an ideal Gaussian beam with a Gaussian tapered vertical array gives a discrepancy in the half-width of 1.7%.

Neither the Gaussian tapered vertical array nor the corresponding Gaussian beam give a Gaussian profile on the horizontal sea surface, as shown in Fig. 9(a). In this figure we show the amplitude in an infinite homogeneous medium at the location of the sea surface. The free surface in the previous example has been removed. This example is similar to Fig. 4 from Zeroug and Felsen (1994). For the Gaussian tapered vertical array the peak amplitude at the interface is at 361.5 m compared to 375 m that would be expected from geometrical optics. The half-width on the left side is 159.0 m compared to 210.8 m for the right side, an eccentricity of 32.5%. However, the left half of the scattering surface (0–375 m) receives essentially the same amount of energy as the right half (375–750 m). For the corresponding Gaussian beam the peak amplitude shifts to only 368.6 m and the eccentricity is only 30.4%. However, the right half of the scattering surface receives 11.1% more energy than the left half.

The phases of the incident beam at the location of the sea surface are shown in Fig. 9(b). To emphasize the discrepancies we show the difference between the phase of the Gaussian beams and the phase of a plane-wave incident at 10° grazing angle. At the surface the phase goes through about 200 periods and the discrepancies are less than a period, that is, less than 0.5%. These phase discrepancies are not the result of numerical approximations or errors. These are the discrepancies in phase of the various Gaussian beams with respect to ideal plane waves.

The grazing angle of a slowly varying field on the horizontal surface can be defined as the inverse cosine of the slope of the phase curve in cycles per wavelength. The phase in radians of a harmonic, plane wave at an angle, α, with respect to a horizontal linear array is $k\cos\alpha x = 2\pi\cos\alpha x/\lambda$, where x is distance along the array, k is wave number, and λ is wavelength. The phase in cycles is $\cos\alpha x/\lambda$, where x/λ is distance along the array in wavelengths. This definition of angle will apply when the field is sufficiently smooth that it can be regarded as locally planar at the surface. For the Gaussian beam case this is not the same as the grazing angle of a geometrical ray. Only the center of a Gaussian beam follows the geometrical ray path. For the tapered vertical array the grazing angle varies from about 7.5° on the left side through a maximum of about 10° to less than 6° on the right side [Fig. 9(c)]. These variations in grazing angle are comparable to the corresponding Gaussian beam.

The optimum, initial half-width of a Gaussian beam propagating 761.57 m in a homogeneous medium ($\omega = 2\pi 400$, $v_0 = 1500$ m/s) is 30.15 m, from Eq. (2). If this value were used for the incident field in the above model (instead of 27.13 m), the half-width of the reflected beam

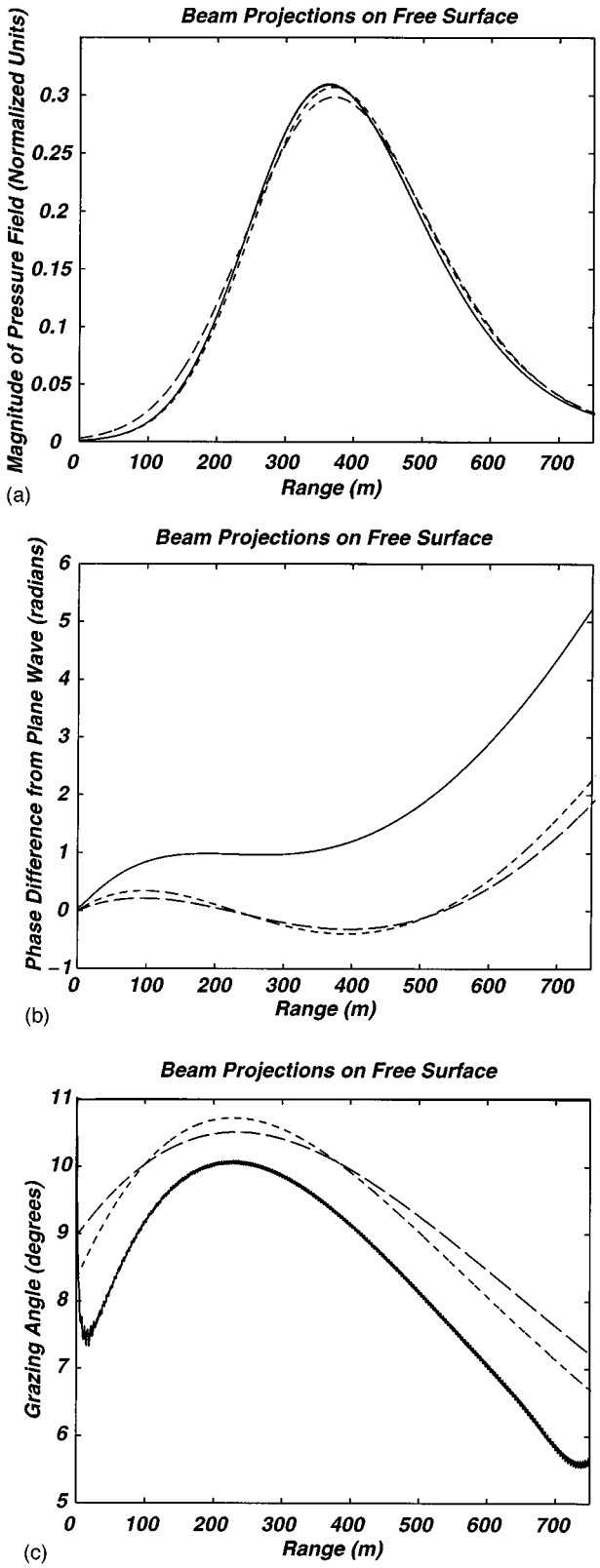

FIG. 9. Neither a Gaussian tapered vertical array (solid line) nor the corresponding Gaussian beam (short dashed line) give a Gaussian profile on the flat sea surface (a). The optimal Gaussian beam (long dashed line) has a more uniform half-width over the surface footprint. To emphasize discrepancies in phase, we show the difference between the phase of the Gaussian beams and the phase of a plane-wave incident on the surface at 10° grazing angle (b). The phase discrepancies are less than a period. The optimal Gaussian beam also has a slightly smaller spread in grazing angle (3°) at the free surface than either the Gaussian tapered vertical array (4.5°) or the corresponding Gaussian beam (4°) (c).

would be 42.64 m (instead of 43.11 m). The optimal beam is not significantly narrower after reflection than the beam actually used. The optimal beam half-width would increase by only 12.49 m (41%) over the propagation path compared to 15.98 m (59%) for the example chosen. However, the optimal beam has a more uniform half-width over the surface footprint [Fig. 9(a)] and a slightly smaller spread in grazing angle (3° vs 4°) [Fig. 9(c)].

III. CONCLUSIONS

The finite-difference solution to test case 1 agrees quite well with the reference solution. Agreement to within 1 dB in amplitude and to within 46° in phase is obtained except for within the steep notch between 193 and 198 m. The mean discrepancy in phase down to 193 m is 13°. Below 193 m we suspect that the reference solution may be incorrect. Twenty points per wavelength are sufficient for acceptable grid dispersion. Also, sea surface heights to a resolution of a twentieth of a wavelength are adequate and finer resolution is not necessary. It is sufficient to specify the sea surface at a range resolution of ten points per wavelength. For the example of sea surface scattering considered here, the details of interpolating roughness at a resolution less than 10 ppw are irrelevant.

The Gaussian tapered vertical array does not generate an exact Gaussian beam. For rigorous scattering problems optimal Gaussian beams should be employed. However, even for optimal Gaussian beams there is significant beamspreading during propagation from the source array to the surface. For an optimal Gaussian beam at 10° grazing angle, as in this paper, the grazing angles at the surface range from about 6° to 10°.

The results reported in this paper were generated using a time-domain, elastic, finite-difference code with the shear terms set to zero. With no additional effort a similar methodology can be applied to pulse beams and seafloor scattering problems from elastic and anelastic bottoms.

ACKNOWLEDGMENTS

I would like to thank Eric Thorsos for providing the reference solution to the sea surface scattering problem addressed in this paper and for many helpful discussions. This work was carried out under Office of Naval Research Grant Nos. N00014-90-J-1493, N00014-95-1-0506, and N00014-96-1-0460. Woods Hole Oceanographic Institution Contribution Number 9252.

Alford, R. M., Kelly, K. R., and Boore, D. M. (**1974**). ''Accuracy of finite-difference modeling of the acoustic wave equation,'' Geophysics **39**, 834–842.

Bamberger, A., Chavent, G., and Lailly, P. (**1980**). ''Etude de schémas numériques pour les équations de l'élastodynamique linéaire'' (41), Rapports de Recherche, Institut National de Recherche en Informatique et en Automatique (INRIA), Domaine de Voluceau, Rocquencourt, 78150 Le Chesnay, France.

Cerjan, C., Kosloff, D., Kosloff, R., and Reshef, M. (**1985**). ''A nonreflecting boundary condition for discrete acoustic and elastic wave equations,'' Geophysics **50**, 705–708.

Červený, V., Popov, M. M., and Pšenčik, I. (**1982**). ''Computation of wavefields in inhomogeneous media: Gaussian beam approach,'' Geophys. J. R. Astron. Soc. **70**, 109–128. Chimenti, D. E., Zhang, J.-G., Zeroug, S., and Felsen, L. B. (**1994**). ''Interaction of acoustic beams with fluid-loaded elastic structures,'' J. Acoust. Soc. Am. **95**, 45–59.

Dablain, M. A. (**1986**). ''The application of high-order differencing to the scalar wave equation,'' Geophysics **51**, 54–66.

Dougherty, M. E., and Stephen, R. A. (**1988**). ''Seismic energy partitioning and scattering in laterally heterogeneous ocean crust,'' Pure Appl. Geophys. **128**, 195–229.

Dougherty, M. E., and Stephen, R. A. (**1991**). ''Seismo/acoustic propagation through rough seafloors,'' J. Acoust. Soc. Am. **90**, 2637–2651.

Felsen, L. B. (**1976**). ''Complex-point-source solutions of the field equations and their relation to the propagation and scattering of Gaussian beams,'' in *Teoria matematica dell'elettromagnetismo, transformazioni, quasiconformi, e questioni connesse*, edited by I.N.D.A.M. (Italy), Vol. 18 (Academic, New York), pp. 39–56.

Higdon, R. L. (**1991**). ''Absorbing boundary conditions for elastic waves,'' Geophysics **56**, 231–241.

Krauss, T. P., Shure, L., and Little, J. N. (**1993**). *Signal Processing Toolbox* (MathWorks, Inc., Natick, MA).

Levander, A. R. (**1985**). ''Use of the telegraphy equation to improve absorbing boundary efficiency for fourth-order acoustic wave finite difference schemes,'' Bull. Seismol. Soc. Am. **75**, 1847–1852.

Levander, A., Harding, A., and Orcutt, J. (**1993**). ''Numerical scattering results for a rough, unsedimented seafloor,'' in *Ocean Reverberation*, edited by D. D. Ellis, J. R. Preston, and H. G. Urban (Kluwer, Dordrecht), pp. 215–220.

Orcutt, J., Harding, A., and Levander, A. (**1993**). ''The effects of seafloor roughness on reverberation: Finite difference and Kirchhoff simulations,'' in *Ocean Reverberation*, edited by D. D. Ellis, J. R. Preston, and H. G. Urban (Kluwer, Dordrecht), pp. 221–226.

Pierson, W. J., and Moskowitz, L. (**1964**). ''A proposed spectral form for fully developed wind sea based on the similarity theory of S. A. Kitaigorodskii,'' J. Geophys. Res. **69**, 5181–5190.

Stephen, R. A. (**1983**). ''A comparison of finite-difference and reflectivity seismograms for marine models,'' Geophys. J. R. Astron. Soc. **72**, 39–57.

Stephen, R. A. (**1990**). ''Solutions to range-dependent benchmark problems by the finite-difference method,'' J. Acoust. Soc. Am. **87**, 1527–1534.

Stephen, R. A., and Swift, S. A. (**1994a**). ''Finite-difference modeling of geoacoustic interaction at anelastic seafloors,'' J. Acoust. Soc. Am. **95**, 60–70.

Stephen, R. A., and Swift, S. A. (**1994b**). ''Modeling seafloor geoacoustic interaction with a numerical scattering chamber,'' J. Acoust. Soc. Am. **96**, 973–990.

Swift, S. A., and Stephen, R. A. (**1994**). ''The scattering of a low-angle pulse beam by seafloor volume heterogeneities,'' J. Acoust. Soc. Am. **96**, 991–1001.

Thorsos, E. I. (**1988**). ''The validity of the Kirchhoff approximation for rough surface scattering using a Gaussian roughness spectrum,'' J. Acoust. Soc. Am. **83**, 78–92.

Thorsos, E. I. (**1996**). ''Test Case 1: Sea surface forward scattering,'' in *Benchmark Solutions in Reverberation and Scattering: Proceedings of the Reverberation and Scattering Workshop*, 2–5 May 1994, edited by D. B. King, S. A. Chin-Bing, J. A. Davis, and R. B. Evans, Naval Research Laboratory Book Contribution NRL/BE/7181-96-001 (U. S. Government Printing Office, Washington, DC), pp. 3.2–3.20.

Virieux, J. (**1986**). ''*P-SV* wave propagation in heterogeneous media: Velocity-stress finite-difference method,'' Geophysics **51**, 889–901.

Zeroug, S., and Felsen, L. B. (**1994**). ''Nonspecular reflection of two- and three-dimensional acoustic beams from fluid-immersed plane-layered elastic structures,'' J. Acoust. Soc. Am. **95**, 3075–3089.